Study of the degradation intermediates formed during electrochemical oxidation of pesticide residue 2,6-dichlorobenzamide (BAM) at boron doped diamond (BDD) and platinum-iridium anodes

Madsen, Henrik Tækker; Søgaard, Erik Gydesen; Muff, Jens

Published in:
Chemosphere

DOI (link to publication from Publisher):
10.1016/j.chemosphere.2014.03.020

Publication date:
2014

Document Version
Publisher's PDF, also known as Version of record

Chemosphere 109 (2014) 84–91

Contents lists available at ScienceDirect

Chemosphere

journal homepage: www.elsevier.com/locate/chemosphere

Study of degradation intermediates formed during electrochemical oxidation of pesticide residue 2,6-dichlorobenzamide (BAM) at boron doped diamond (BDD) and platinum–iridium anodes

Henrik Tækker Madsen *, Erik Gydesen Søgaard, Jens Muff *

Department of Biotechnology, Chemistry and Environmental Engineering, Aalborg University, Niels Bohrs Vej 8, 6700 Esbjerg, Denmark

HIGHLIGHTS

- 2,6-Dichlorobenzamide is efficiently degraded by direct electrochemical oxidation.
- Degradation occur via hydroxylation and dechlorination until ring opening.
- BDD leads to lower amounts of stable intermediates compared to Pt–Ir.
- Combining HPLC/ESI–MS, HPLC–UV and TOC is powerful for intermediate studies.

ARTICLE INFO

Article history:
Received 19 November 2013
Received in revised form 4 March 2014
Accepted 6 March 2014

Handling Editor: E. Brillas

Keywords:
Pesticide pollution
Electrochemical oxidation
Degradation intermediates
Groundwater
2,6-Dichlorobenzamide

ABSTRACT

Electrochemical oxidation is a promising technique for degradation of otherwise recalcitrant organic micropollutants in waters. In this study, the applicability of electrochemical oxidation was investigated concerning the degradation of the groundwater pollutant 2,6-dichlorobenzamide (BAM) through the electrochemical oxygen transfer process with two anode materials: Ti/Pt_{90}–Ir_{10} and boron doped diamond (Si/BDD). Besides the efficiency of the degradation of the main pollutant, it is also of outmost importance to control the formation and fate of stable degradation intermediates. These were investigated quantitatively with HPLC–MS and TOC measurements and qualitatively with a combined HPLC–UV and HPLC–MS protocol. 2,6-Dichlorobenzamide was found to be degraded most efficiently by the BDD cell, which also resulted in significantly lower amounts of intermediates formed during the process. The anodic degradation pathway was found to occur via substitution of hydroxyl groups until ring cleavage leading to carboxylic acids. For the BDD cell, there was a parallel cathodic degradation pathway that occurred via dechlorination. The combination of TOC with the combined HPLC–UV/MS was found to be a powerful method for determining the amount and nature of degradation intermediates.

1. Introduction

Electrochemical oxidation (EO) is a technology within the family of Advanced Oxidation Processes (AOPs) used for treatment of aqueous non-biodegradable recalcitrant organic pollutants of high toxicity through oxidation by primarily, but not exclusively, highly reactive hydroxyl radicals (Comninellis et al., 2008). In recent years, the electrochemical oxidation water treatment technology has developed from fundamental research on synthesis of new electrode materials aimed at high oxidation power, resistance and durability and laboratory studies of treatment efficiencies of various industrial wastewaters and other polluted aqueous matrices into commercial available products utilizing boron-doped diamond (BDD) and the more traditional platinum based and dimensionally stable (DSA) mixed oxides anodes (Comninellis et al., 2008; Anglada et al., 2009; Panizza and Cerisola, 2009). Concurrent to the incipient market dissemination of the technology, much more research is still needed in order to fully understand the effect of the technology on the water matrices and the produced effluents. One challenge is elucidating degradation pathways of parent organic pollutants and identifying oxidation intermediates with the aim of ensuring final discharge of an environmentally safe effluent. Generalization of the degradation pathways for different organic contaminants has despite of similarities proved to be challenging, and laboratory studies targeting the individual contaminants are typically needed (Boye et al., 2006; Comninellis et al., 2008; Cavalcanti et al., 2013).

* Corresponding authors. Tel.: +45 20960733 (H.T. Madsen). Tel.: +45 99403564 (J. Muff).
E-mail addresses: htm@bio.aau.dk (H.T. Madsen), jm@bio.aau.dk (J. Muff).

http://dx.doi.org/10.1016/j.chemosphere.2014.03.020
0045-6535/

One contaminant in need of AOPs for effective and fast removal is the pesticide transformation product (PTP) 2,6-diclorobenzamide (BAM). BAM is a daughter product of the commonly used pesticide dichlorobenil, formed during the percolation of dichlorobenil to groundwater aquifers, and is the main contaminant found in Danish groundwater resources. Of the total number of groundwater aquifers that are included in the Danish groundwater monitoring program, 50% have been found to be contaminated with pesticides and PTPs, and in 18.8–20.2% of these cases, the primary contaminant is BAM (Thorling et al., 2012). BAM has been found to be a persisting pollutant. Although its use was banned in 1996, concentrations in the groundwater have not decreased significantly, and it is expected to be present in the aquifers for many years (Thorling et al., 2012). Removal of BAM is therefore necessary before the water can be consumed, but traditional Danish drinking water treatment has been shown to be ineffective against BAM and most other pesticides and PTPs (Søgaard et al., 2001). This makes BAM an obvious candidate for an AOP treatment, but so far no such study has been undertaken.

1.1. Electrochemical oxidation mechanisms

In the EO process, the organics are oxidized by a combination of two different processes, the electrochemical oxygen transfer process (EOTR) and indirect bulk oxidation. In the EOTR process, the organics are oxidized by intermediates of oxygen evolution with the first step being the discharge of water to form adsorbed active oxygen species; physisorbed hydroxyl radicals in the case of non-active anodes (1) or chemisorbed active oxygen in the case of active anodes (2), where a stronger adsorption of the hydroxyl radicals promotes a further removal of an electron (Comninellis, 1994; Kapałka et al., 2009).

$$MO_x + H_2O \rightarrow MO_x(\cdot OH) + H^+ + e^- \quad (1)$$

$$MO_x(\cdot OH) \rightarrow MO_{x+1} + H^+ + e^- \quad (2)$$

The sorbed reactive oxygen species are then capable of partial organic oxidation (in the case of MO_{x+1}) (3) and or full combustion (in the case of $MO_x(\cdot OH)$) (4). The decomposition of the active oxygen species into molecular oxygen is the main competitive side reaction (5) that lowers the efficiencies (Comninellis, 1994).

$$MO_{x+1} + R \rightarrow MO_x + RO + H_2O + H^+ + e^- \quad (3)$$

$$MO_x(\cdot OH) + R \rightarrow MO_x + CO_2 + H_2O + H^+ + e^- \quad (4)$$

$$MO_{x+1}/MO_x(\cdot OH) \rightarrow MO_x + 1/2O_2(+H^+ + e^-) \quad (5)$$

In the indirect mediated organic oxidation process, electroactive ions or other solution constituents are oxidized at the anode surface in order to produce strong oxidants capable of bulk chemical oxidation (Panizza and Cerisola, 2009). In particular, chloride has proved to be an efficient mediator in the indirect oxygen transfer process in chloride rich media through the oxidation of chloride to hypochlorous acid/hypochlorite active chlorine species ((6) and (7), with an initiation potential of 1.64 V versus SHE or higher) or through adsorbed oxychloro-species (8) and (9) (Bonfatti et al., 2000).

$$2Cl^- \rightarrow Cl_2 + 2e^- \quad (6)$$

$$Cl_2 + H_2O \rightarrow HOCl + H^+ + Cl^- \rightleftharpoons OCl^- + 2H^+ + Cl^- \quad (7)$$

$$MO_x(\cdot OH) + Cl^- \rightarrow MO_x(HOCl)_{ads} + e^- \quad (8)$$

$$MO_x(HOCl)_{ads} + R \rightarrow CO_2 + H_2O + Cl^- \quad (9)$$

The classification of different electrode materials into the classes of active and non-active anodes is based on their overpotentials for oxygen evolution, where a high overpotential results in a high hydroxyl radical production and higher mineralization efficiency. Classification of common electrode materials have been performed by the group of Comninellis (Comninellis et al., 2008; Kapałka et al., 2009), who presents boron doped diamond (BDD) as the limit of the non-active anodes and DSA anodes as the limit of the active anodes. Non-active anodes generally present the highest efficiencies considering the EOTR and have usually been found to be superior concerning rate of reaction and mineralization efficiency (Sirés et al., 2008; Samet et al., 2010; Malpass et al., 2013).

1.2. Aim of study

The aim of this study was to elucidate the degradation pathway of BAM treated by EO through the EOTR oxidation mechanism, and from this work develop a generalized evaluation procedure for studies of degradation pathways. Identification of intermediate species formed and their fate during the oxidation process is essential in order to evaluate the risk of formation of harmful byproducts that potentially can results in an increase in effluent toxicity. Identifying the degradation intermediates (DIs) of one pollutant can also be used in transferring the gained knowledge to similar contaminants. For reasons of comparison between active and non-active anodes two different electrochemical cells are used utilizing Si/BDD and Ti/Pt–Ir anodes. The latter platinum–iridium anode material is considered to belong primarily to the active anode class of electrode materials even though some hydroxyl radical formation can be expected.

2. Materials and methods

2.1. Chemicals

2,6-Dichlorobenzamide, 3,5-dichlorophenol, 2,4-dichlorobenzoic acid, 4-chlorobenzoic acid, benzoic acid, maleic acid and oxalic acid were all purchased at Sigma Aldrich with purity >98%. Methanol and acetonitrile (HPLC grade) were purchased from VWR. Demineralized water was produced in house with a Silex II ion exchanger from SILHORKO. Stock solutions of 100 mg L^{-1} were prepared in acetonitrile.

2.2. Electrochemical oxidation setup and procedure

The electrochemical oxidation was performed galvanostatically in a batch recirculation setup. An illustration of the setup can be found in a previous work (Muff et al., 2012). For each experiment, 3 L of model solution was pumped from a water cooled reservoir through the electrochemical cells. Two different commercial one-compartment electrochemical cells with different anode materials were applied. One of tubular design from Watersafe S.A. (Greece) with an internal cylindrical anode of titanium coated with platinum alloyed with iridium ($Ti/Pt_{90}–Ir_{10}$), with a total anode surface area of 60.3 cm^2 and the cathode comprising the outer walls of the cell made of stainless steel AISI 316 with an internal diameter of 42 mm. The electrode gap in the cell was 6 mm. The BDD cell was obtained from Adamant Technologies S.A. (Switzerland), a DiaCell type 100 cell with 70.0 cm^2 silicon coated boron doped diamond (Si/BDD) anode and corresponding cathode mounted as plates with a 3 mm electrode gap in between. The flow rate in the system was kept constant at 430 L h^{-1} and the applied current density were 50 mA cm^{-2} obtained by applied currents of 3.0 and 3.5 A for the two cells, respectively. The different geometry of the two cells induced different hydrodynamics that might

influence the efficiency. However, the hydrodynamics of both cells were evaluated at the applied flow rate of 430 L h^{-1}. Reynolds number calculations showed that the flow in both cells were in the laminar flow regime (Watersafe: 1052 and DiaCell: 1322) and mass transfer estimations by the diffusion limiting current technique showed that the mass transfer coefficients of both cells were similar (Watersafe: $k_m = 1.54 \times 10^{-5}$ m s^{-1} and DiaCell: $k_m = 1.47 \times 10^{-5}$ m s^{-1}, determined in previous work (Muff et al., 2012). The similar mass transfer coefficients were important, since they directly influence anode surface reactions. Based on this evaluation, the two cells were considered comparable with respect to this study.

As model solutions, 300 mg BAM was dissolved in 3 L demineralized water (100 mg L^{-1}) with 42.6 g (100 mM) of sodium sulfate added as supporting electrolyte. The solution was left stirring for at least 24 h prior to each experimental run for complete BAM dissolution. The experiments were operated at a constant temperature of 25 °C and with cell potentials of 4.7 V for the Pt–Ir cell and 8.1 V for the BDD cell. Sampling occurred from the reservoir for the aqueous analysis at specific time intervals.

2.3. Analytical procedures

The degradation of BAM and the formation of intermediate products were analyzed with a HPLC/UV/ESI–MS system (1260 Infinity and 1100 series LC/MSD Trap, Agilent Technology), equipped with a ZORBAX Eclipse Plus C18 column. A 40:60 (v/v) mixture of methanol and ammonium acetate buffer (pH 3) was used as eluent, and pumped with a flow rate of 400 μL min^{-1} at 25 °C. The UV detector was set at 225 nm. On the ESI–MS, the nebulizer pressure was set at 2.76 bar, the nebulizer flow at 9 L min^{-1}, and the dry gas temperature to 350 °C. Nitrogen was used for nebulization and dry gas. The spectra were recorded in positive mode. For quantitative determination of compounds, tandem mass spectroscopy was applied.

The extent of mineralization of organic matter in the samples was investigated by determining total organic carbon (TOC) in the aqueous samples with a multi N/C 2100 analyzer from Analytik Jena, and the total UV absorbance was determined with a Cary 50, Varian.

2.4. Procedure for determination of intermediates

To elucidate the chemical structure of DIs, the UV and MS detector on the HPLC were used in combination. Separately, each technique suffers from a number of drawbacks. The UV detector cannot be used for qualitative investigation of a peak unless a reference standard is used. The MS, with the electrospray interface, is influenced by the ionic content of the sample matrix, which eluates in the beginning of the analysis, where also smaller molecules such as organic acids and small amides will eluate. Together the two techniques can overcome these drawbacks to some degree. It is often easier to detect a peak with the UV detector due to the much more stable background signal/base line, and by knowing the retention time of a peak, the peak can be qualitatively analyzed using the MS. Also, because the sample matrix has no UV absorbance, the UV detector may be used to investigate the formation of smaller and fast eluating compounds. In our study, the general procedure was to observe peaks with the UV detector to determine retention times, after which the mass of the molecule responsible for the peak was determined with MS.

To support the analysis, reference compounds were used. This made it possible to study how specific changes to the molecular structure of the molecules influenced the retention times with our specific column and eluent composition. The main aims of these analyses were to study the effect of replacing the amide group with a carboxylic acid group, and the effect of the dechlorination process on the retention times.

3. Results and discussion

3.1. Degradation of BAM

As seen in Fig. 1, the degradation of BAM was found to follow first order kinetics for both cells with apparent rate constants of $k_{BDD} = 8.5 \times 10^{-3}$ min^{-1} ($R^2 = 0.997$) and $k_{Pt-Ir} = 4.6 \times 10^{-3}$ min^{-1} ($R^2 = 0.991$) obtained with an applied current density of 50 mA cm^{-2}. The difference in the rate constants was enlarged by the larger anode area of the BDD cell resulting in an increased current intensity, and the two kinetic parameters were more appropriately compared with respect to the specific amount of charge in ampere hours per liter passed through the solution instead of minutes. After this normalization the constants became: $k_{BDD} = 4.4 \times 10^{-1}$ $(Ah\ L^{-1})^{-1}$ and $k_{Pt-Ir} = 2.8 \times 10^{-1}$ $(Ah\ L^{-1})^{-1}$. Overall this shows that the BDD cell was more efficient at degrading BAM compared to the Pt–Ir cell.

A more markedly difference in the two processes was found when the total UV absorbance of the solutions during the EO process was compared, Fig. 2. Initially, both spectra were characterized by a small peak from 270 to 280 nm, minimum absorbance at 250 nm and a sharp increase in absorbance around 225 nm, just before absorption by the water solvent. To get a better impression of the variations in the UV absorbance spectra the specific absorbance at 225, 254 and 270 nm were plotted in the inset plots in Fig. 2. 225 and 254 nm were chosen since they represent wavelengths at which UV absorbance of organics are often evaluated, and 270 nm was chosen in order to follow the development of the initial minor peak in the original BAM spectrum.

For the Pt–Ir cell no immediate drop in UV intensity was seen. The absorbance around 225 nm was relatively constant up until 240 min (4 Ah L^{-1}), and at the same time the absorbance at higher wavelengths was found to increase, as seen from the inset in Fig. 2a. Only after 240 min did the absorbance begin to decrease.

The BDD cell was much more efficient at reducing the total absorbance. The peaks at 225 and 270 nm did immediately decrease, and the increase in the absorbance around 254 nm was much smaller compared to the increase seen for the Pt–Ir anode and it began to decrease already after 120 min (2.3 Ah L^{-1}).

Together with the degradation of BAM, these UV absorbance data indicated that the electrochemical processes of the BDD cell

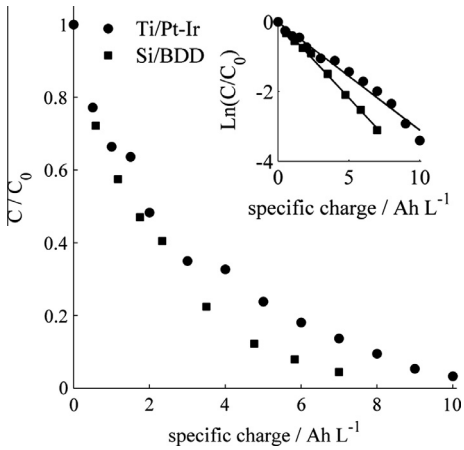

Fig. 1. Degradation kinetics for BAM during electrochemical oxidation by two different cells with Si/BDD and Ti/Pt–Ir as anode materials at 50 mA cm^{-2}. (a) Concentration of BAM versus time and (b) concentration of BAM versus specific charge.

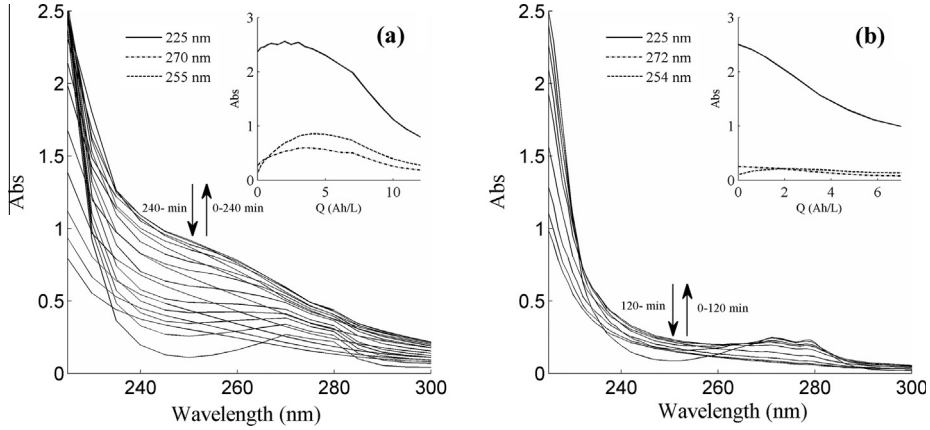

Fig. 2. Evolution in the UV spectrum of the solution during the EO process. (a) The Pt–Ir cell and (b) the BDD cell.

was much more efficient in complete BAM mineralization, whereas the processes at the Pt–Ir anode initially converted BAM to other UV absorbing compounds through partial oxidation. This difference of the two cells was expected and fits with the general understanding of the oxidation power and processes occurring during electrochemical oxidation of other organic contaminants, and has now been documented for BAM.

3.2. Quantification of degradation intermediates

To quantify the DIs formed during the process, the TOC concentration of the solutions was measured during the runs. A fast TOC removal from the solution would indicate efficient mineralization of BAM in the process, and in light of the UV absorption results, differences in the performance of the cells were expected. As seen in Fig. 3, the BDD cell did show a faster removal of TOC compared to the Pt–Ir cell with first order rate constants $k_{BDD} = 5.2 \times 10^{-3}\ min^{-1} = 2.7 \times 10^{-1}\ (Ah\ L^{-1})^{-1}$ ($R^2 = 0.992$) and $k_{Pt-Ir} = 1.2 \times 10^{-3}\ min^{-1} = 7.1 \times 10^{-2}\ (Ah\ L^{-1})^{-1}$ ($R^2 = 0.963$).

When the TOC data were combined with the BAM degradation data, it allowed for a determination of the total amount of organic carbon bound in DIs. The amount of DI carbon was calculated by determination of the area between the TOC curve and the curve representing the concentration of BAM related carbon calculated from the BAM degradation data. The evolution in the DI carbon (the grey area) was then plotted with respect to the specific charge passed through the solution as the insets in Fig. 4. As the subplots clearly show, much more BAM was completely mineralized near

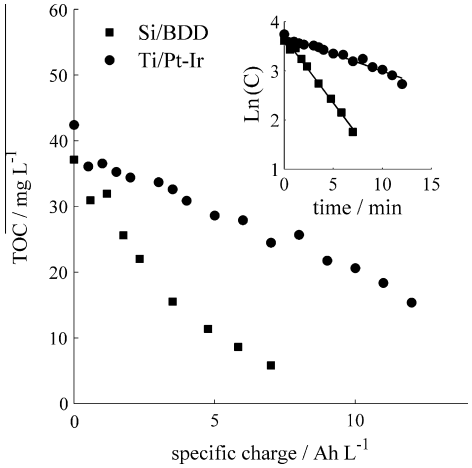

Fig. 3. TOC removal for the two cells with first order kinetic inset plot.

the surface of the BDD anode compared to the Pt–Ir anode. With the Pt–Ir cell, the level of stable DIs in the solution reached a level of 54% after 5.7 Ah L^{-1}, as represented by the amount of original carbon in the solution bound in intermediates (Fig. 4b), whereas the same number for the BDD cell only reached 20% after 3.0 Ah L^{-1} (Fig. 4a).

This difference observed in the amount of stable DI formed between the two cells was directly related to the oxidation power of the two anode materials. The BDD acted as a non-active anode where the hydroxyl radicals produced on the anode surface will have a sufficient high standard reduction potential for oxidation of both BAM and DIs. The Pt–Ir material is in the transition between active and non-active, but with predominant behavior as an active anode, where the chemisorbed oxygen will oxidize BAM more selectively due to the lower reduction potential. The unselective nature of the hydroxyl radicals from the BDD anode ensured that, when BAM was oxidized to a DI, the main part of the DI (80%) was subsequently further oxidized until complete mineralization.

The flow regime in the cells could also have an influence on the amount of DI produced during the treatment. For an effective mass transport of organics to the electrode surface, hydrodynamics providing turbulent conditions are often demanded for high faradaic yield (Mascia et al., 2010; Cordeiro et al., 2013). On the contrary, laminar flow in the cell could potentially minimize the DI formation. Results indicating this hypothesis were found by Mascia et al. (2010), although not highlighted because focus was on the overall rate of removal, which typically is the standard evaluation parameter. The reason for the lower amounts of DIs at laminar flow may be that under these conditions the transport of DIs from surface to bulk will primarily be diffusive. Therefore DIs will tend to stay in close proximity of the surface, where they are more likely to undergo further oxidation. A conceptual model of the BAM oxidation under laminar conditions is that BAM was degraded to its first DI at the entrance of the cell, after which this DI moves further along the surface until it reaches the outlet of the cell or undergoes complete mineralization. This potential influence of flow on the intermediate compound formation will be studied in detail in coming research.

Finally, the more selective nature of the chemisorbed active oxygen in the Pt–Ir cell ensured that BAM was preferentially degraded relative to its DIs, providing the observed accumulation of DIs seen in Fig. 4b.

3.3. Efficiency of the degradation process

Another way of comparing the efficiency of the two cells in mineralizing BAM was through the mineralization current efficiency

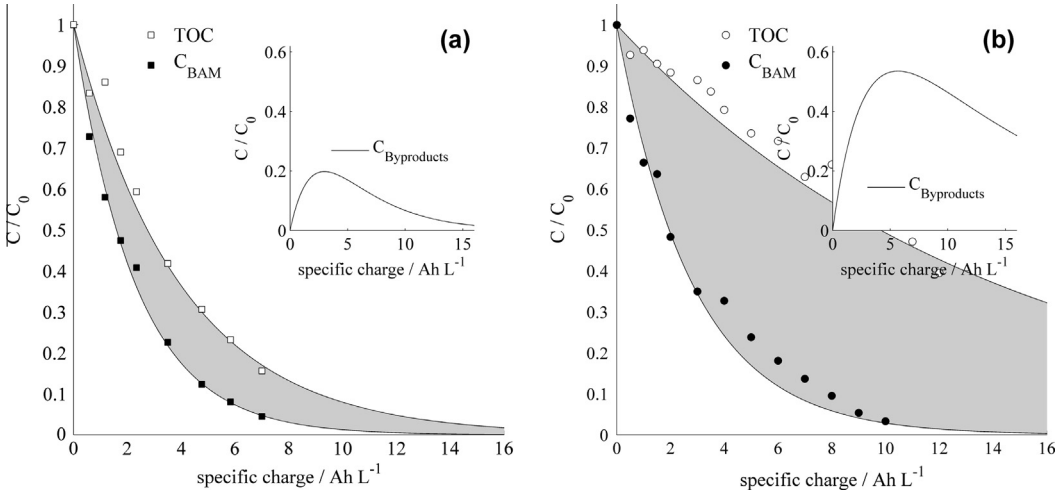

Fig. 4. Combined plots of TOC and BAM related carbon for determination of the total amount of DI bound carbon. (a) The results obtained with the BDD cell, and (b) the results obtained with the Pt–Ir cell. $C_{0,BAM}$ = 100 mg L^{-1}.

(MCE). The overall mineralization reaction of BAM could be written as follows:

$$C_7H_5ONCl_2 + 16H_2O \rightarrow 7CO_2 + NO_3^- + 2Cl^- + 37H^+ + 34e^- \quad (10)$$

This reaction showed that 34 electrons were involved in incinerating a BAM molecule completely into carbon dioxide. Due to the cost of electricity, current efficiency is an important parameter in electrochemical oxidation, and the MCE at a given time can be comparatively calculated using the experimental TOC data and the relationship (Brillas et al., 2004; Yoshihara and Murugananthan, 2009):

$$MCE = \frac{\Delta(TOC)_{exp}}{\Delta(TOC)_{theo}} \cdot 100 \quad (11)$$

$\Delta(TOC)_{exp}$ denotes the experimentally determined TOC removal in the time interval Δt $(t + \Delta t - t)$ in g L^{-1}. $\Delta(TOC)_{theo}$ is the theoretically TOC removal considering that all electrical charge is consumed to yield reaction (11) calculated as follows:

$$\Delta(TOC)_{theo} = \frac{I_{app} \cdot M_C \cdot \Delta t}{F \cdot V \cdot ne} \quad (12)$$

I_{app} is the applied current intensity in C s^{-1}, M_C is the molar mass of carbon of 12 g mol^{-1}, Δt is the time interval in seconds, F is the Faraday constant of 96 490 C mol^{-1}, V is the volume in L and ne is the average number of electrons needed per carbon atom in BAM for its incineration (34/7 mol electrons per mole carbon).

The same procedure can be used to calculate the MCE with respect to the removal of BAM itself as parent product applying 189 g mol^{-1} as the molar mass of BAM and 34 electrons for its incineration in the calculation of the theoretical BAM removal.

In Fig. 5 the experimentally determined MCE for both anode materials is plotted for both BAM and TOC as a function of the specific charge. To investigate the fit of the MCE model, the theoretically MCEs is also plotted. These values are calculated from the derivatives to the exponential 1. Order BAM and TOC removal curves seen in Figs. 1 and 3.

In general, the MCEs were highest in the start of the process (up to 17%) where the total concentrations of organics were at its maximum providing the best probability for an efficient transport to the anode surface. The importance of the concentration on the MCE is shown in the insets in Fig. 5, where the MCEs were plotted as a function of the respective BAM and TOC concentration. At very low concentrations, the MCE became accordingly low. For the initial concentrations applied in this study, still more than 80% of the current in the circuit originated from oxygen liberation or other unwanted waste side reactions, but this can be improved by increasing the concentration of a given pollutant prior to degradation, and by decreasing the applied current density. Highest MCEs were seen by the BDD cell, and due to smaller quantity of DIs formed using this cell, the efficiency of the BAM and TOC removal was more alike compared to the Pt–Ir cell, where the slow TOC removal resulted in a low average efficiency in the range of 2–3% and a poor fit to the model due to higher analytical uncertainties.

3.4. Identification of degradation intermediates

In the evaluation of the potential risk of the DIs formed during the electrochemical oxidation process, it is not sufficient to look at the total quantity of DIs formed. The specific chemical nature of the DIs also has to be studied. In Table 1, retention times of peaks detected in the samples during the EO process are shown. The general procedure was to search for peaks with the UV detector and then determine the mass and intensity of the compound responsible for the peak with the mass spectrometer. For the very fast eluating peaks, it was not possible to obtain identification with the mass spectrometer.

It is interesting to note that there was a distinct difference in the DIs formed with the two cells, see Fig. 6. Quantification of the specific DIs through calibration of the intensities with concentrations was not possible due to the lack of calibration standards, so the height of the peaks for the different DIs cannot be compared. What could be compared was the sequence of appearance. For the Pt–Ir cell, the mother compound, BAM (190 m/z), was first converted to a daughter product with an m/z value of 206, which then was further converted into a compound with a m/z value of 188. The intensities of the DIs reached a maximum after 6 Ah L^{-1} and then decreased rapidly until they were beyond detection in the last sample. For the BDD cell, the 206 m/z peak was also seen. However, with this cell, it was not possible to find the 188 m/z peak. Instead, peaks at 156 m/z and 122 m/z were detected. These two peaks increased rapidly and reached a maximum intensity after 1 Ah L^{-1}. It may also be noted that the increase and decrease of these peaks coincided with development of the UV intensity as seen in Fig. 2.

As a tool for assisting with elucidating the chemical structure of the DIs, the retention times of known reference compounds with active groups similar to what was likely for the daughter products

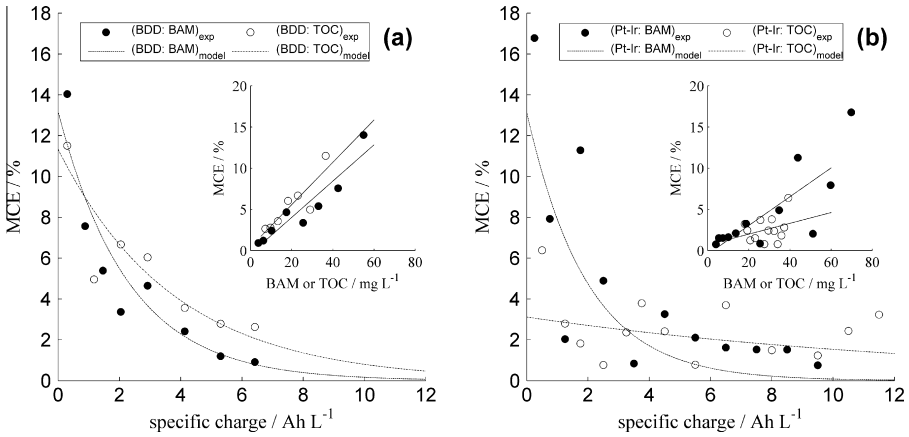

Fig. 5. The mineralization current efficiency (MCE) as a function of the specific charge deposited with respect to BAM and TOC respectively. (a) The BDD cell and (b) the Pt–Ir cell. Data points represent experimentally collected data, and the curves represent theoretical values determined from previously determined removal kinetics. The inset plots show the correlation between concentration and the MCE.

Table 1
Comparison of peaks detected during oxidation with the two electrochemical cells and standard compounds representing specific changes in the molecular structure. (+) For the UV detector in the BDD experiment, refers to the fact that this compound was poorly separated from the dominating BAM peak with the analytical separation method applied in this study. The peak was however easily observed in tandem mass spectrometry.

EO solution					Standard compounds		
Retention time (min)	BDD		Pt–Ir		Standard	MS m/z (+/−)	Retention time (min)
	MS (m/z)	UV (225 nm)	MS (m/z)	UV (225 nm)			
0.91	–	+	–	+	Oxalic acid	91/89	0.88
1.15	–	–	188	+	Maleic acid	117/115	0.99
1.40	206	+	206	+	Benzoic acid	223/221	5.11
1.79	122	+	–	–	2,4-Dichlorobenzoic acid	191/189	14.3
1.90	156	(+)	–	–	4-Chlorobenzoic acid	157/155	16.3
2.02	190	+	190	+	3,5-Dichlorophenol	163/161	48.0

were measured, see Table 1. From the comparison of the retention time of BAM with the retention time of 2,4-dichlorobenzoic acid and 3,5-dichlorophenol, it was clear that a loss or conversion of the amide group should result in markedly prolonged retention times for the DIs. As this was not seen in our spectra, it indicated that the amide group was not affected by the oxidation in either of the two cells. Table 1 also shows that loss of two chloro groups will lower the retention time, while the loss of only one of the chloro groups will have a less significant influence on the retention time. This is most probably due to the change in polarity induced by the changes in molecular structure, and it seemed reasonable to assume that as the polarity increased the retention time decreased. Lastly, Table 1 shows that small carboxylic acids were poorly retained by the applied column and eluated almost immediately.

Together with the masses of the peaks, these considerations indicated that the peaks at 206 and 188 m/z were BAM molecules, where the EO process has resulted in the first step a substitution of one hydroxyl group with a hydrogen atom (16 Da mass difference) and in the second step substitution of a chlorine atom with another hydroxyl group (18 Da mass difference). Substitution with hydroxyl groups has also been observed by others working with the degradation of aromatic compounds (Boye et al., 2006; Borràs et al., 2010; Wei et al., 2011; Rabaaoui et al., 2013), and seem to constitute the initial steps of the degradation. Based on steric considerations, the first substitution will probably occur on C4. The presence of a hydroxyl group will increase the polarity, and as predicted from the experiments with the reference compounds, the retention time of the 206 m/z peak was markedly shorter than the retention time of BAM. The 188 m/z peak was found to appear after the 206 m/z peak, which indicated that it was formed from the 206 m/z compound. Again the increased polarity of the 188 m/z compound was in accordance with the observed decrease in retention time.

The two additional peaks detected in the BDD experiment had masses lower than BAM, but with only weakly decreased retention times. The difference in mass was equal to the reductive loss of first one and then two chloro groups. It therefore seemed that for the BDD cell, there existed two parallel degradation pathways: an anodic and a cathodic, whereas only the anodic pathway was active for the Pt–Ir cell.

Based on the experimental findings, a pathway for the initial electrochemical degradation steps of BAM was proposed and is depicted in Fig. 6.

There are some unknowns. Firstly, the 188 m/z compound was not detected in the BDD experiment. However, as was shown in Fig. 4, the total amount of DIs was much lower when using the BDD cell compared to the Pt–Ir cell and furthermore, the amount of DIs for the BDD cell was the composite of the anodic and cathodic pathways. For the Pt–Ir cell the intensity of the 188 m/z peak was considerably lower than the signal of the 206 m/z peak, and the absence of the 188 m/z peak in the BDD experiment could therefore very well be due to a concentration below the detection limit. Secondly, a compound with a protonated mass of 170 Da has been proposed in the reaction scheme although this compound has not been observed. However, based on the experiments with the reference compounds, the amide group has not been found to be affected, and the next logical step of the anodic process would therefore be to continue the chloro/hydroxy substitution before any ring cleavage occurs. Due to its polarity, the 170 m/z compound would eluate even faster than the 188 m/z compound, which would bring it to eluate with the supporting electrolyte,

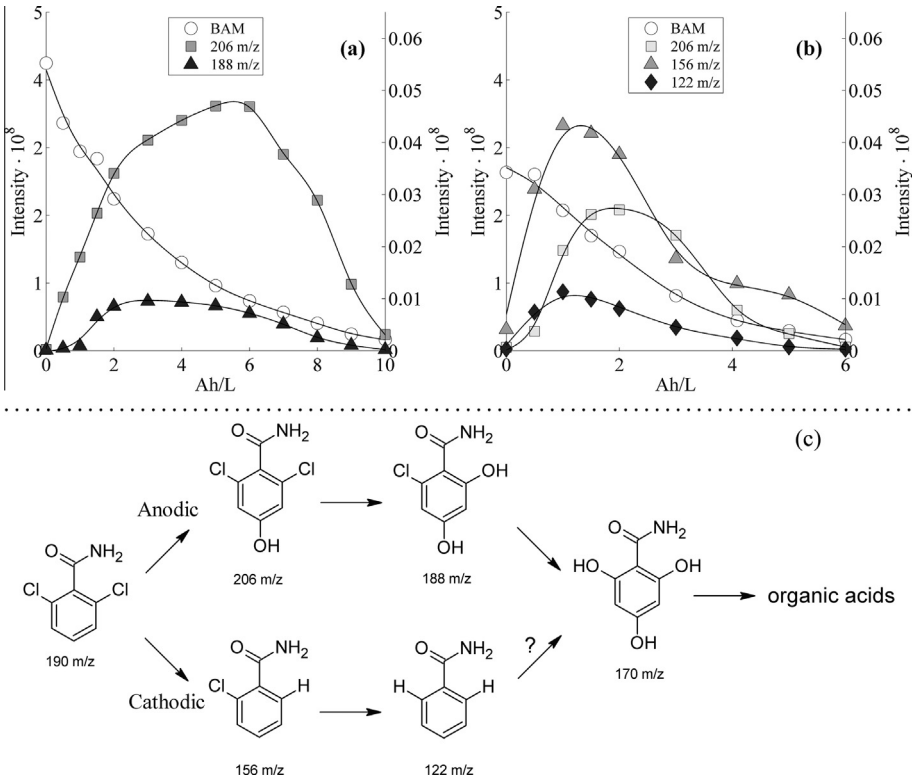

Fig. 6. Development in intensity of degradation intermediates detected with mass spectrometer and proposed pathway for the initial electrochemical degradation of BAM. The subplots (a and b) represent the experiments with the Pt–Ir cell (a) and the BDD cell (b). Intensities for the DIs are plotted on the right *y*-axis and the intensity of BAM on the left. Subplot (c) is the proposed degradation pathway. The cathodic pathway was only found to be active for the BDD cell, and although it was not found in the experiments, we suggest that this reaction pathway leads to the same hydroxylated ring structure (170 *m*/*z*) as for the anodic pathway.

and thereby make detection with the mass spectrometer impossible because of the dominating influence of the electrolyte ions. Different eluent mixtures were tried to investigate if a better separation could be obtained, but on the column used in these experiments that was not possible.

For the same reasons the peak at 0.91 min could not be identified either. It does however seem likely that the 0.91 min peak represented carboxylic acids formed in the process due to aromatic ring cleavage. This has been shown in other reported studies with electrochemical oxidation of similar aromatic compounds (Boye et al., 2006). Although of scientific interest, the specific nature of the carboxylic acids is of less interest from a practical point of view, since these compounds carry little toxicity and are readily biodegradable. With that said however, it is important to note that we did not find any transformation of the amide group, and the toxicity of small amides could pose a potential problem (Friedman, 2003). However, if present the concentrations were low and below the detection limit of the TOC.

3.5. Generalized protocol for determine of DIs

As shown in this manuscript, a protocol for determination of DIs should consist of two parts, an estimation of the total quantity of DIs and the specific chemical nature of these. For the first part, a degradation plot of the original pollutant and TOC can be used to effectively estimate the total amount of organic carbon in DIs. A simpler way is to measure the total UV absorbance, but this approach cannot to be used to quantify the amount of DIs, and is more appropriately used to compare different degradation processes. For the qualitative investigation, the combined technique of UV and mass spectrometry is very useful. Peaks are more easily found with the UV detector due to a stable base line, and it does not suffer from the interference of the supporting electrolyte. As seen in this study, a mass spectrometer with an electrospray interface will not be able to detect compounds that eluate at the same time as the supporting electrolyte. With the retention time determined, the mass spectrometer can be employed to investigate the nature of the compound further. Since the general effect of the EO process was to increase the polarity of the DIs, the choice of column on the HPLC is very important. It may be necessary to apply a second column to handle small polar compounds.

4. Conclusions

2,6-Dichlorobenzamide was found to be degraded by both electrochemical cells in the study utilizing respectively Si/BDD and Ti/Pt–Ir as anode materials representing a non-active anode type and a predominal active anode material. The BDD cell was found to be the most efficient, and it also resulted in the lowest amount of degradation intermediates formed during the process, which was ascribed to the unselective nature of the hydroxyl radicals formed at this high oxidation power anode. The total quantity of DIs in the solution during the treatment was estimated by subtracting the degraded amount of BAM related carbon from the TOC.

The initial degradation pathway was found to be different for the two cells. The BDD gave rise to both a cathodic and an anodic pathway, whereas the Pt–Ir cell only followed the anodic pathway. In the anodic pathway, first a hydrogen atom was substituted with a hydroxyl group, after which the chloro groups were substituted with hydroxyl groups. In the cathodic pathway, the chloro groups were substituted with hydrogen atoms. The final step was cleavage of the aromatic ring structure leading to unidentified carboxylic acids.

The combination of UV and mass spectrometer was found to be an effective combination for detecting and identifying the DIs.

Acknowledgements

Financial support from the Danish Ministry of Science, Technology, and Innovation in the form of a Ph.D. study grant is acknowledged.

References

Anglada, Á., Urtiaga, A., Ortiz, I., 2009. Contributions of electrochemical oxidation to waste-water treatment: fundamentals and review of applications. J. Chem. Technol. Biotechnol. 84, 1747–1755.

Bonfatti, F., Ferro, S., Lavezzo, F., Malacarne, M., Lodi, G., De Battisti, A., 2000. Electrochemical incineration of glucose as a model organic substrate II. Role of active chlorine mediation. J. Electrochem. Soc. 147, 592–596.

Borràs, N., Oliver, R., Arias, C., Brillas, E., 2010. Degradation of atrazine by electrochemical advanced oxidation processes using a boron-doped diamond anode. J. Phys. Chem. A 114, 6613–6621.

Boye, B., Brillas, E., Marselli, B., Michaud, P., Comninellis, C., Farnia, G., Sandona, G., 2006. Electrochemical incineration of chloromethylphenoxy herbicides in acid medium by anodic oxidation with boron-doped diamond electrode. Electrochim. Acta 51, 2872–2880.

Brillas, E., Boye, B., Sirés, I., Garrido, J.A., Rodríguez, R.M., Arias, C., Cabot, P.-L., Comninellis, C., 2004. Electrochemical destruction of chlorophenoxy herbicides by anodic oxidation and electro-Fenton using a boron-doped diamond electrode. Electrochim. Acta 49, 4487–4496.

Cavalcanti, E.B., Garcia-Segura, S., Centellas, F., Brillas, E., 2013. Electrochemical incineration of omeprazole in neutral aqueous medium using a platinum or boron-doped diamond anode: Degradation kinetics and oxidation products. Water Res. 47, 1803–1815.

Comninellis, C., 1994. Electrocatalysis in the electrochemical conversion/combustion of organic pollutants for waste water treatment. Electrochim. Acta 39, 1857–1862.

Comninellis, C., Kapalka, A., Malato, S., Parsons, S.A., Poulios, I., Mantzavinos, D., 2008. Advanced oxidation processes for water treatment: advances and trends for R & D. J. Chem. Technol. Biotechnol. 83, 769–776.

Cordeiro, G.S., Rocha, R.S., Valim, R.B., Migliorini, F.L., Baldan, M.R., Lanza, M.R.V., Ferreira, N.G., 2013. Degradation of profenofos in an electrochemical flow reactor using boron-doped diamond anodes. Diamond Relat. Mater. 32, 54–60.

Friedman, M., 2003. Chemistry, biochemistry, and safety of acrylamide. A review. J. Agric. Food Chem. 51, 4504–4526.

Kapałka, A., Fóti, G., Comninellis, C., 2009. The importance of electrode material in environmental electrochemistry: formation and reactivity of free hydroxyl radicals on boron-doped diamond electrodes. Electrochim. Acta 54, 2018–2023.

Malpass, G.R.P., Salazar-Banda, G.R., Miwa, D.W., Machado, S.A.S., Motheo, A.J., 2013. Comparing atrazine and cyanuric acid electro-oxidation on mixed oxide and boron-doped diamond electrodes. Environ. Technol. 34, 1043–1051.

Mascia, M., Vacca, A., Polcaro, A.M., Palmas, S., Ruiz, J.R., Da Pozzo, A., 2010. Electrochemical treatment of phenolic waters in presence of chloride with boron-doped diamond (BDD) anodes: experimental study and mathematical model. J. Hazard. Mater. 174, 314–322.

Muff, J., Jepsen, H., Søgaard, E., 2012. Bench-scale study of electrochemical oxidation for on-site treatment of polluted groundwater. J. Environ. Eng. 138, 915–922.

Panizza, M., Cerisola, G., 2009. Direct and mediated anodic oxidation of organic pollutants. Chem. Rev. 109, 6541–6569.

Rabaaoui, N., Saad, M.E.K., Moussaoui, Y., Allagui, M.S., Bedoui, A., Elaloui, E., 2013. Anodic oxidation of o-nitrophenol on BDD electrode: variable effects and mechanisms of degradation. J. Hazard. Mater. 250–251, 447–453.

Samet, Y., Agengui, L., Abdelhédi, R., 2010. Electrochemical degradation of chlorpyrifos pesticide in aqueous solutions by anodic oxidation at boron-doped diamond electrodes. Chem. Eng. J. 161, 167–172.

Sirés, I., Brillas, E., Cerisola, G., Panizza, M., 2008. Comparative depollution of mecoprop aqueous solutions by electrochemical incineration using BDD and PbO_2 as high oxidation power anodes. J. Electroanal. Chem. 613, 151–159.

Søgaard, E.G., Aruna, R., Abraham-Peskir, J., Koch, C.B., 2001. Conditions for biological precipitation of iron by gallionella ferruginea in a slightly polluted ground water. Appl. Geochem. 16, 1129–1137.

Thorling, L., Hansen, B., Langtofte, C., Brüsch, W., Møller, R.R., Mielby, S., 2012. Grundvand: Status og Udvikling 1989–2011 (groundwater: Status and Development 1989–2011). Technical report, Geological Survey of Denmark and Greenland, 2012.

Wei, J., Feng, Y., Sun, X., Liu, J., Zhu, L., 2011. Effectiveness and pathways of electrochemical degradation of pretilachlor herbicides. J. Hazard. Mater. 189, 84–91.

Yoshihara, S., Murugananthan, M., 2009. Decomposition of various endocrine-disrupting chemicals at boron-doped diamond electrode. Electrochim. Acta 54, 2031–2038.